ACS APPLIED MATERIALS & INTERFACES

Research Article

www.acsami.org

Semiconducting Polymer Encapsulated Mesoporous Silica Particles with Conjugated Europium Complexes: Toward Enhanced Luminescence under Aqueous Conditions

Jixi Zhang,*[,†,‡] Neeraj Prabhakar,[‡,§] Tuomas Näreoja,[§] and Jessica M. Rosenholm*[,‡]

[†]Key Laboratory of Biorheological Science and Technology, Ministry of Education, College of Bioengineering, Chongqing University, Chongqing 400044, China

[‡]Laboratory of Physical Chemistry, Åbo Akademi University, 20500 Turku, Finland

[§]Laboratory of Biophysics, Faculty of Medicine, University of Turku, 20520 Turku, Finland

Supporting Information

ABSTRACT: Immobilization of lanthanide organic complexes in meso-organized hybrid materials for luminescence applications have attracted immense interest due to the possibility of controlled segregation at the nanoscopic level for novel optical properties. Aimed at enhancing the luminescence intensity and stability of the hybrid materials in aqueous media, we developed polyvinylpyrrolidone (PVP) stabilized, semiconducting polymer (poly(9-vinylcarbazole), PVK) encapsulated mesoporous silica hybrid particles grafted with Europium(III) complexes. Mono-silylated β-diketonate ligands (1-(2-naphthoyl)-3,3,3-trifluoroacetonate, NTA) were first co-condensed in the mesoporous silica particles as pendent groups for bridging and anchoring the lanthanide complexes, resulting in particles with an mean diameter of ~450 nm and a bimodal pore size distribution centered at 3.5 and 5.3 nm. PVK was encapsulated on the resulted particles by a solvent-induced surface precipitation process, in order to seal the mesopores and protect Europium ions from luminescence quenching by producing a hydrophobic environment. The obtained polymer encapsulated MSN-EuLC@PVK-PVP particles exhibit significantly higher intrinsic quantum yield (Φ_{Ln} = 39%) and longer lifetime (τ_{obs} = 0.51 ms), as compared with those without polymer encapsulation. Most importantly, a high luminescence stability was realized when MSN-EuLC@PVK-PVP particles were dispersed in various aqueous media, showing no noticeable quenching effect. The beneficial features and positive attributes of both mesoporous silica and semiconducting polymers as lanthanide-complex host were merged in a single hybrid carrier, opening up the possibility of using these hybrid luminescent materials under complex aqueous conditions such as biological/physiological environments.

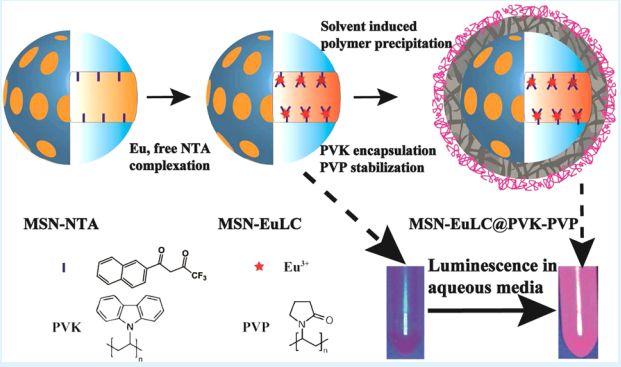

KEYWORDS: *mesoporous silica particles, Europium complex, semiconducting polymer, hybrid material, photoluminescence*

INTRODUCTION

Lanthanide(III) complexes have attracted a tremendous amount of research efforts due to their excellent luminescence properties as optical probes/labels. They possess large Stokes' shifts, long emission lifetimes (micro- to milliseconds range), and well-defined narrow emission peaks, which allows for discrimination against background autofluorescence associated with commonly used organic fluorophores in chemical biology. Research into lanthanide-doped organic−inorganic hybrid materials emerged in the 1990s with the development of interesting materials for advanced optical applications such as fiber amplifiers and solid-state high-efficiency lasers.[1−4]

A rational design and a better control of the local structures of these hybrid materials, as well as their degrees of organization, are important issues, especially if tailored photophysical properties are sought. The interest in using mesoporous silica particles as the host for the hybrid materials stems from the attractive properties of mesoscopically ordered porous structures, such as high surface areas, tunable pore sizes, large accessible pore volumes, and controlled segregation at the nanoscopic level, which allow for the immobilization of a large number of well-separated guest molecules per particle.[5−7] Although still at the early stages of the development, they have emerged as one of the most appealing host materials for organic lanthanide complexes in the past decade.[1] Moreover, mesoporous silica derived hybrid materials exhibit great potential in photonics, as they are transparent, have high thermal stability, and substantial mechanical strength. Generally, covalent binding of the complexes to the silica host is particularly attractive among various preparation strategies, and

Received: July 30, 2014
Accepted: October 7, 2014
Published: October 7, 2014

superior to physical impregnation techniques due to a low risk of chelate release and cluster induced self-quenching.[1,4] Hence, many research efforts have been dedicated to the incorporation of silylated anchoring ligands (i.e., β-diketones) on the mesopore walls by the co-condensation method to achieve high homogeneity and ascertain enough coupling amount of the complexes.[8−14] With these advantages notwithstanding, the photoluminescence of these hybrid materials was studied in the solid state, or as solutions in organic solvents in the past. Additionally, challenges still remain in the fabrication of hybrid particles with carefully controlled particle size and well-defined particle morphology for applications in the fields of biolabeling and bioimaging.

As lanthanide ions generally possess a coordination number of nine, the widely used bidentate antenna ligands often lead to hexa-coordinated trislanthanide complexes inside the mesoporous silica host. Hence, the inner coordination sphere of lanthanide ions is not fully saturated, which is completed by coordination of some water or solvent molecules. To address this challenge, some auxiliary neutral coligands with suitable triplet energy levels, such as bipyridine,[15] phenanthroline,[10,14,16] and polymers,[9,17] were extensively used in previous studies to substitute these water or solvent molecules. Nevertheless, the coordination bonds inside the lanthanide complexes are not strong enough to prevent the luminescence change under the influences from the environmental species, which is, however, the design rationale of the biosensors, bioanalytics for ions or molecules on the basis of lanthanide-doped organic−inorganic hybrid materials.[18−20] To develop imaging or diagnostics probes, stable and long-term luminescence of lanthanide complexes inside the host is typically preferred. In the field of using polymers as the host materials, pioneering work on polymer particles incorporated with lanthanide complexes has demonstrated that hydrophobic polymers can efficiently enwrap the complexes to achieve bright and stable luminescence.[21,22] There has also been considerable progress in semiconducting polymer coated inorganic nanoparticles for enhancing fluorescence brightness and photostability.[23,24] It may then appear a bit surprising that very few detailed studies have been performed that aim at sealing the mesoporous channels or encapsulate the host particle by strategies like surface coating methods.

In light of the above-mentioned considerations, we herein present a novel kind of hybrid material consisting of semiconducting polymer encapsulated mesoporous silica particles with conjugated Europium complexes. Emphasis is first put on the preparation of hybrid mesoporous silica particles with well-defined particle morphology by the co-condensation route, as well as well-organized Europium complex immobilization. Subsequently, our focus will be on the encapsulation of these particles by semiconducting polymer (poly(9-vinylcarbazole), PVK) to seal the mesopores and protect the Europium complexes from quenching by the hydrophilic species in the aqueous media. Detailed characterization of the photoluminescence properties of the as-prepared materials is shown. The significant enhancement in photoluminescence achieved by polymer encapsulation is demonstrated and highlighted. The potential of employing the as-prepared hybrid particles for time-resolved microscopy imaging is presented.

EXPERIMENTAL SECTION

Chemicals. Unless otherwise noted, all reagent-grade chemicals were used as received, and Millipore water was used in the preparation of all aqueous solutions. Polyvinylpyrrolidone (PVP, MW 90 000) was purchased from ACROS. Cetylmethylammonium bromide (CTAB, AR) was purchased from Fluka. Anhydrous tetrahydrofuran (THF), anhydrous ethanol (AR), 2-propanol (AR), tetraethyl orthosilicate (TEOS, AR), 3-chloropropyltrimethoxysilane (AR), NH_4OH (30 wt %, AR), 1-(2-naphthoyl)-3,3,3-trifluoroacetonate (NTA), sodium hydride, $EuCl_3{\cdot}6H_2O$, and poly(9-vinylcarbazole) were purchased from Sigma.

Preparation of 1-(2-Naphthoyl)-3,3,3-trifluoroacetonate (NTA) Derived Organosilane (NTA-Si). Monosilylated NTA derivative (NTA-Si) was synthesized by reacting 3-chloropropyltrimethoxysilane with NTA according to the procedures published in the previous studies. Subsequently, 0.167 mmol (44.3 mg) of NTA was dissolved in 4 mL of anhydrous tetrahydrofuran (THF) under stirring. Thereafter, 0.167 mmol (4 mg) of sodium hydride was added and the mixture was stirred for 90 min at room temperature. Then, 0.167 mmol (31 μL) of 3-chloropropyltrimethoxysilane was added dropwise. Thereafter, the mixture was heated to 65 °C and the reaction was maintained by stirring under nitrogen atmosphere overnight. The solvent was evaporated by using a rotary evaporator, and the product was dissolved in diethyl ether. The resulting solution was evaporated, leading to the yellow oil compound NTA-Si ($C_{20}H_{23}F_3O_5Si$, MW: 429). FT-IR (KBr, cm^{-1}): 3104 ν_{as}(C−H); 2925 $\nu_{as}(CH_2,CH_3)$; 2857 $\nu_s(CH_2,CH_3)$; 1621 ν(C−O); 1561 ν(C−O, C−C); 1280 $\nu(CF_3)$; 1244 ν(C−Si); 1191 and 1065 ρ(Si−O−CH_3); 800 ν(Si−O); 470 δ(Si−O−Si). ^{1}H NMR (δ ppm, $CDCl_3$): 0.5−0.8 (m, 2H, CH_2 (2)); 1.7−1.9 (m, 2H, CH_2 (3)); 3.3−3.5 (m, 2H, CH_2 (4)); 3.68 (s, 9H, CH_3 (1)); 6.22 (t, 1H, CH (5)); 7.0−8.6 (m, 7H, naphthalenyl).

Synthesis of NTA-Si Modified Mesoporous Silica Nanoparticles (MSN-NTA). The MSN-NTA particles, where the organic NTA ligands were incorporated in the inorganic silica matrix, were prepared by the co-condensation procedure using TEOS and NTA-Si as the silica source according to the modified protocol reported by us.[25] In a typical experimental procedure for MSN-NTA, first a mixed solution was prepared by dissolving and heating CTAB (0.45 g) in a mixture of water (150 mL) and ethylene glycol (18 mL) at 70 °C in a flask reactor. Ammonium hydroxide (30 wt %, 2.5 mL) was introduced to the system as a catalyst before TEOS (1.5 mL) and NTA-Si (in 2 mL ethanol) were added to initiate the reaction. The molar ratio used in the synthesis was 1 TEOS:0.19 NTA-Si:0.18 CTAB:5.9 NH_3:53.1 2-propanol:1249 H_2O. The reaction was allowed to proceed for 3 h at 70 °C. Then, the stirring was stopped and the as-synthesized colloidal suspension was then aged at 70 °C for 24 h. After the suspension was cooled to room temperature, the suspension was separated by centrifugation (10000 rpm, 20 min).

The template removal for all as prepared MSN-NTA particles was performed by a highly efficient ion-exchange method.[26] The purified nanoparticles were redispersed in a solution containing 60 mg of ammonium nitrate in 20 mL of ethanol, and then the mixture was stirred at 60 °C for 30 min. The procedure was repeated three times to completely remove the surfactants. The final product was suspended in ethanol for further use.

Synthesis of Eu Complexes Functionalized Mesoporous Hybrid Material (MSN-EuLC). The preparation of MSN-EuLC was carried out by anchoring of Eu^{3+} by MSN-NTA and subsequent coordinating free NTA ligands to complete the coordination sphere of Eu^{3+}, according to the procedures described in the literature.[13] In a typical process, 50 mg of MSN-NTA was dispersed in an ethanol solution of $EuCl_3{\cdot}6H_2O$ (7.7 mg in 10 mL, with a molar ratio of Eu:NTA-Si being 1:1) under stirring. Then, 44 μL triethylamine was added and the mixture was stirred for 2 h. Afterward, a NTA solution in ethanol (11 mg in 1 mL, with a molar ratio of Eu:NTA being 1:2) was added to complete the coordination sphere of Eu^{3+}. The mixture was stirred at room temperature for 10 h, and the obtained particles were recovered by centrifugation (6000 rpm, 15 min) and washing with ethanol. The final luminescent product was suspended in ethanol for further use.

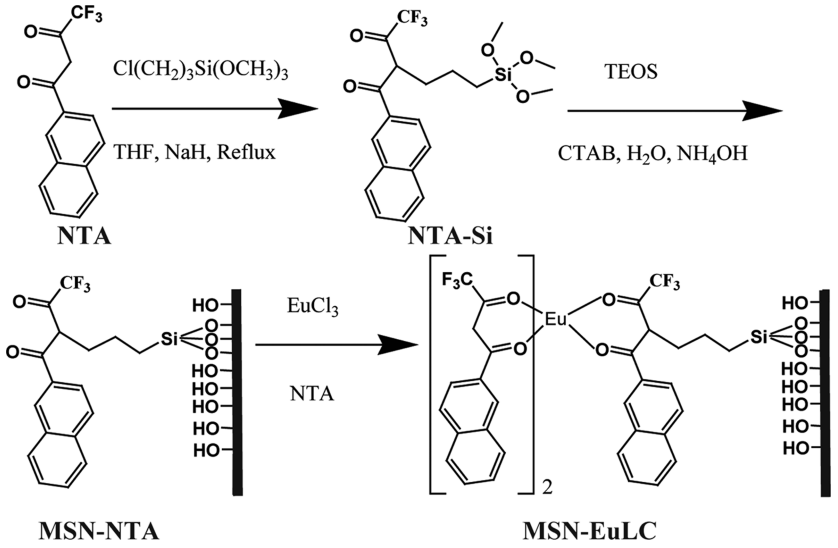

Figure 1. Schematic representation for the preparation of monosilylated NTA ligand (NTA-Si), MSN particles co-condensed with NTA-Si (MSN-NTA), and Eu-ligand complex loaded MSN particles (MSN-EuLC).

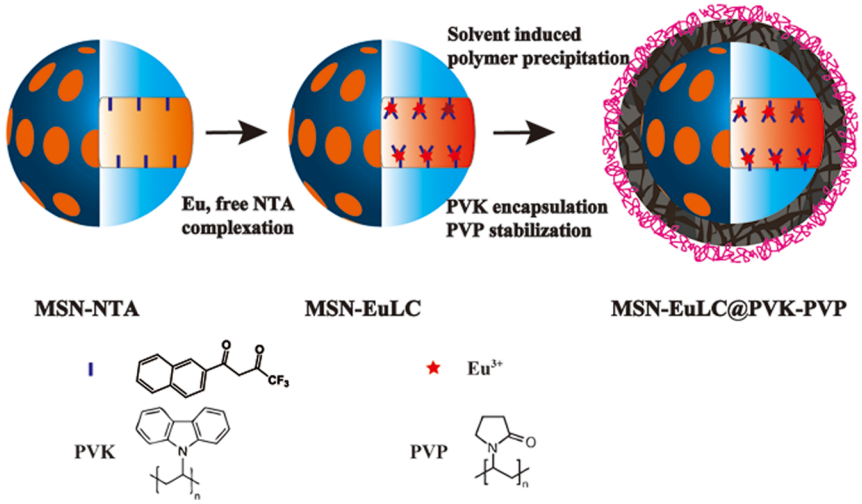

Figure 2. Schematic representation for the formation of Eu-ligand complex loaded MSN particles (MSN-EuLC) and PVP stabilized PVK encapsulated MSN-EuLC particles (MSN-EuLC@PVK-PVP). Solvent induced PVK precipitation on the surface of MSN-EuLC was carried out in the mixture of THF and ethanol, facilitated by sonication. PVP was employed as a stabilizer in the synthesis in order to avoid particle aggregation in solutions.

Encapsulation of MSN-EuLC Particles with Semiconducting Polymer. The encapsulation of MSN-EuLC particles with semiconducting PVK polymer was conducted according to a nanoprecipitation method[21] with some modifications. Typically, 2 mg of the as-prepared MSN-EuLC particles was mixed with 0.5 mL of PVK solution in anhydrous THF (2 mg/mL). Then the mixture was added dropwise to a polyvinylpyrrolidone (PVP) solution in anhydrous ethanol (1 mg/mL, 2.5 mL) under sonication. During the addition and sonication, the color of the suspension turned much whiter. Afterward, the mixture was stirred for 2 h at room temperature. The as-obtained particles (denoted as MSN-EuLC@PVK-PVP) were retrieved by centrifugation (6000 rpm, 15 min) and washed with 4-(2-hydroxyethyl)-1-piperazineethanesulfonic acid (HEPES) buffer (pH 7.2, 25 mM) three times to remove free polymers. Finally, the particles were suspended in HEPES buffer for further use.

Particle Characterizations. Transmission electron microscopy (TEM) images were obtained by a JEM 1400-Plus (JEOL, Japan) instrument with a 120 kV acceleration voltage. Scanning electron microscopy (SEM) measurements were performed with a Zeiss DSM 962 microscope operated at an accelerating voltage of 10.0 kV. X-ray diffraction (XRD) measurements were performed using a Kratky compact small-angle system (Hecus Braun, Austria) as described in our previously published paper.[27] The hydrodynamic size distributions of the samples were measured using dynamic light scattering (DLS) techniques by a Zetasizer Nano instrument (Malvern, UK) at 25 °C. Nitrogen sorption isotherms were measured with a ASAP2010 analyzer (Micromeritcs, Norcross, GA, USA). The specific surface areas were calculated by the Brunauer–Emmett–Teller (BET) method[28] in a linear relative pressure range between 0.05 and 0.25. The pore size distributions were derived from the desorption branches of the isotherms by the non localized density functional theory (NLDFT) method[29] using NLDFT kernel file developed for silica exhibiting a cylindrical pore geometry. The Fourier transform infrared (FT-IR) spectra were collected over the range of 4000–400 cm^{-1} on a Spectrum 100 infrared spectrophotometer (PerkinElmer, Waltham, MA, USA) using a KBr technique. Fluorescence spectra for the particle suspensions were measured by a LS 50B fluorescence spectrometer (PerkinElmer, Waltham, MA, USA). Thermogravimetric analysis (TGA) was conducted with a TG 209 instrument (NETZSCH, Exton, PA, USA). The materials were tested under an air atmosphere from 30 to 900 °C at a heating rate of 10 °C/min. Luminescence

lifetimes were measured at room temperature by using a Cary Eclipse fluorescence spectrophotometer. The absolute luminescence quantum yields (Φ_{abs},%) were measured by a relative method designed for lanthanide complexes, using 10 nM Eu^{3+} in the Wallac DELFIA Enhancement Solution (molar absorption coefficient 37 500, quantum yield 70%) as a standard.[30] The luminescence decay curves obtained during measuring the luminescence lifetimes were used to calculate the quantum yield, in order to circumvent the influence of concentration and particle scattering on the determination which was found in emission-based calculations. The detailed calculation methods were shown in the Supporting Information.

Time-Resolved Microscopy Imaging. Time-resolved microscopy images of particles were recorded using a time-resolved fluorescence microscope prototype (Signifer, PerkinElmer Life Science, Wallac Oy, Finland), a standard fluorescence microscope (Nikon Eclipse E600, Tokyo, Japan) equipped with the attachment for time-resolved fluorescence imaging, including a xenon flash lamp (pulse length 10 μs; pulse energy, 0.1 J/pulse; frequency, 500 Hz), a chopper, timing electronics and a cooled charge-coupled device (CCD) camera (UltraPix TE3/A/S, EG&G Wallac, Turku, Finland).[31,32] The filter block used for imaging of Eu complexes contained the following components: excitation filter, DUG11 (Schott Glaswerke, Mainz, Germany); emission filter, 615/7.5 nm (BARR Associates Inc., Westford, MA, USA); dichroic mirror, 400 DCLP (Nikon Corp., Tokyo, Japan). The delay time and the gate time of the time-resolved detection were 100 and 800 μs, respectively. The integration time was 30 s. Particles from a stock solution of 0.2 mg/mL (in HEPES buffer, pH 7.2) were dropped and dried on glass microscope slides prior to microscopic examination.

RESULTS AND DISCUSSION

Characterization of MSN-NTA and MSN-EuLC. The synthesis procedures for the silylated β-diketonate ligand (NTA-Si), MSN particles co-condensed with NTA-Si (MSN-NTA), and Europium complex loaded MSN particles (MSN-EuLC) are shown in Figures 1 and 2. The employed 3-chloropropyltrimethoxysilane reacts with NTA to produce a hydrolyzable sol–gel precursor NTA-Si, which can be introduced onto the surface of MSN by the co-condensation method, and subsequently function as the pendent bridging agent between the Europium complex and the inorganic mesoporous silica host. The structure of the modified ligand (NTA-Si) was confirmed by ^{1}H NMR ($CDCl_3$) and FT-IR spectra (Figure S1 of the Supporting Information). The hydrogen atom signal in the α-position of diketone is observed at 6.22 ppm in ^{1}H NMR, as expected for the methylene group from the monosilylation on NTA.

Typical transmission electron microscopy (TEM) and scanning electron microscopy (SEM) images of the as-synthesized MSN-NTA particles are shown in Figure 3a,b. A relatively uniform morphology of spherical particles was observed, with a mean particle size of around 450 nm. The TEM image clearly shows mesoporous channels with a number of notable voids dispersed irregularly amid the mesoporous framework. Thermogravimetric curve of MSN-NTA under an air atmosphere (Figure 4a) shows a distinct wide stage of weight loss from 150 to 800 °C (13 wt %), which should be mainly resulted from the decomposition of organic matter. The amount of monosilylated NTA (NTA-Si) in the material was calculated to be around 0.42 mmol/g based on this weight loss. In the FT-IR spectrum (Figure 4b), two peaks at 2925 and 2857 cm^{-1} originated from the methylene groups of NTA-Si are observed in MSN-NTA material, which indicates that the NTA groups were successfully anchored on the MSN surfaces by the co-condensation method.

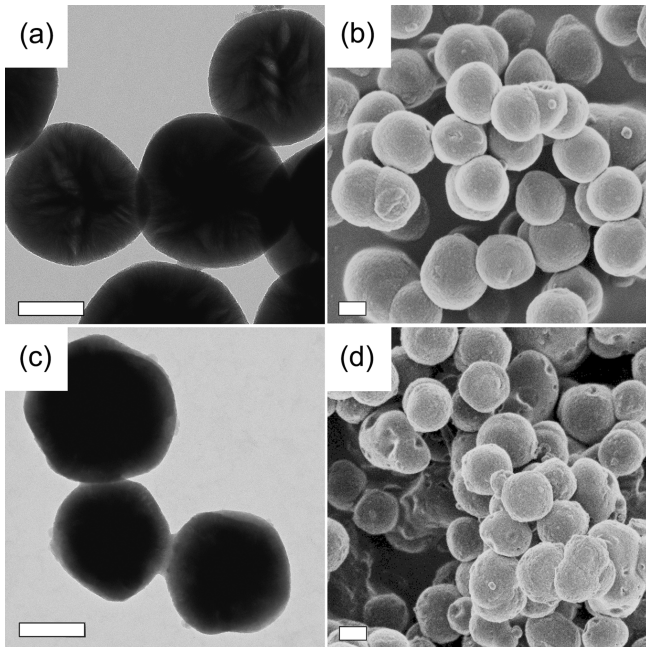

Figure 3. TEM and SEM images of MSN-NTA particles (a and b), and MSN-EuLC@PVK-PVP particles (c and d). Scale bar represents 200 nm.

Nitrogen sorption analysis of MSN-NTA (Figure 4c) displays a typical type-IV isotherm pattern with a sharp capillary condensation step at relative pressures (P/P_0) in the range of 0.2–0.4, indicating that the material has one-dimensional cylindrical mesopore channels with an pore size distribution peak at 3.5 nm (Figure 4d inset). The specific surface area and pore volume of MSN-NTA are determined to be 915 m^2/g and 0.67 cm^3/g, respectively, as shown in Table 1. In addition to the capillary condensation step at low P/P_0, a uncommon type-H4 hysteresis loop at P/P_0 values between 0.4 and 0.9 was observed. This hysteresis revealed another peak at 5.3 nm in the pore size distribution curve. Taking into account the voids observed in the TEM image, it is highly possible that the hysteresis is associated with the effects of pore blocking around the embedded slit-shaped voids in the mesoporous framework of MSN-NTA material. Hence, the generated MSN-NTA particles possess bimodal pore size distribution resulting from the mixture of the pore structures. The mechanism for the generation of void defects in the co-condensation approach is complicated and it may differ from one case to the other, depending on the type and concentration of organosilane in the synthesis.[33−36] In the case of NTA-Si, the aromatic rings and the aliphatic chain render high hydrophobicity to the silane. Considering the possible interaction between the cationic headgroup of CTA^+ and NTA by the π-cation interaction,[37] the incorporation of NTA silane in MCM-41 synthesis would lead to the change of cylindrical micelles to more complex aggregates, and in turn, results in the formation of the void defects in MSN-NTA particles.

In the previous studies where silylated β-diketonate was used to covalently immobilize lanthanide complex in the mesoporous host, a postgrafting/functionalization strategy was widely employed,[1,3,38,39] whereas very few succeeded in forming uniform hybrid nanoparticles by the co-condensation method.[13] Considering that a better segregation degree of the ligand groups facilitates brighter luminescence in the host,[3] the

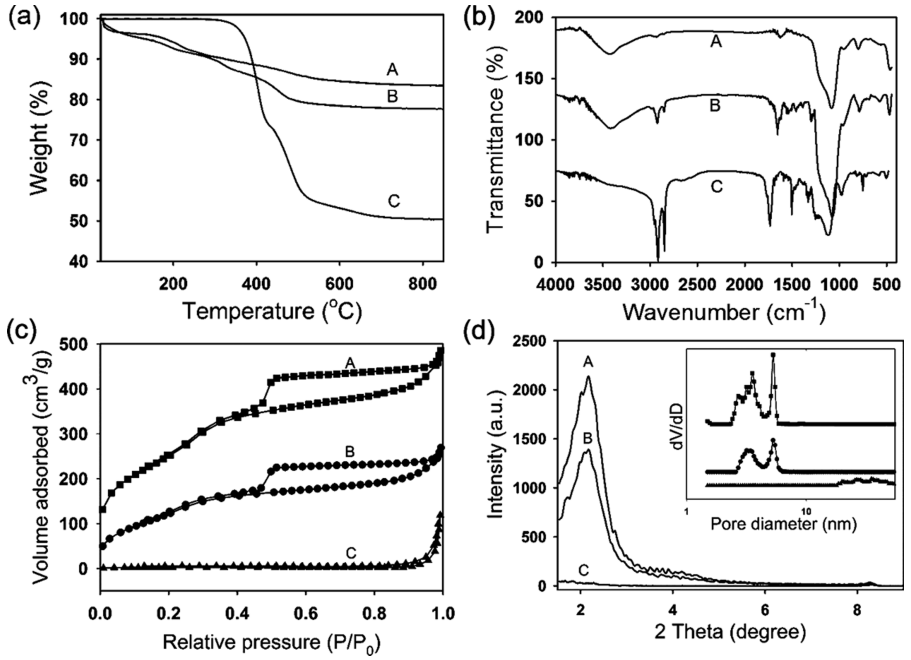

Figure 4. TGA curves (a), FT-IR spectra (b), nitrogen sorption isotherms (c), and small angle XRD patterns (d) of MSN-NTA (A), MSN-EuLC (B), and MSN-EuLC@PVK-PVP (C). Inset of (d) is the corresponding pore size distributions deduced from the desorption branches of nitrogen sorption isotherms.

Table 1. Textural Parameters of MSN-NTA, MSN-EuLC, MSN-EuLC@PVK-PVP

	S_{BET} (m^2/g)	C-value	V_p (cm^3/g)	D_{NLDFT} (nm)
MSN-NTA	915	76	0.67	3.5, 5.3
MSN-Eu(NTA)3	472	32	0.36	3.3, 5.3
MSN-Eu(NTA)3@PL	50	97		

co-condensation approach is more advantageous. Herein, it is worth mentioning the unique role of 2-propanol in the success of our co-condensation synthesis. Although synthesis in the presence of methanol or ethanol suffered from either irregular particle morphology or low surface area and pore size (Figure S2 of the Supporting Information), 2-propanol allowed the formation of MSN-NTA with well-defined particle morphology and pore structure. It is conceivable that a more thermodynamically favored coassembly process was facilitated in the case of lower polarity 2-propanol rather than in methanol or ethanol, regarding the hydrophobicity and molecular structure of NTA-Si.

By anchoring the Eu^{3+} by complexation with free NTA and the co-condensed NTA-Si ligands, MSN-EuLC particles were obtained. The TEM image of MSN-EuLC (Figure S3 of the Supporting Information) indicates that the particle morphology and mesostructures were intact after the complexation process. A 19 wt % weight loss of MSN-EuLC from 150 to 800 °C in the corresponding TGA curve corresponds to an increase of 0.22 mmol of NTA per gram of the material. If we assume that each Eu^{3+} was coordinated by 3 NTA in MSN-EuLC,[13] as shown in Figure 1, there was 0.11 mmol of bound ligand (NTA-Si) per gram of MSN-NTA accessible for the bridging of Eu complex by the coordination of Eu^{3+} and free NTA ligand. A substantial decrease in the nitrogen sorption amount of MSN-EuLC reveals a significant drop of the surface area (to 472 m^2/g) and the pore volume (to 0.36 cm^3/g), which should be attributed to the occupation of the pore space by the anchored complexes. The intensity of the main peak of the small angle XRD pattern (Figure 4d) becomes weaker after the complexation step, arising from the decrease in the electron density discrepancy between the silica pore wall and the pore space. Characteristic stretching vibration of the enol tautomer form of β-diketonate can be observed at 1621 cm^{-1} ($\nu_{C=O}$) and 1561 cm^{-1} ($\nu_{C=C}$) with fine and intense bands in the FT-IR spectrum of MSN-EuLC (Figure 2b), further confirming the coordination of the complexes in the MSN host.[40,41]

Notably, the complexation in the particles resulted in a substantial decrease in the C-values derived from the BET method (from 76 in the case of MSN-NTA to 32 in the case of MSN-EuLC), which indicates a remarkable decrease in the surface polarity originated from the increased amount of NTA ligands in the particles.[27,42] The increased surface hydrophobicity of the particles could facilitate the encapsulation of particles by hydrophobic polymers in the next step.

Characterization of MSN-EuLC@PVK-PVP. MSN-EuLC particles were encapsulated by semiconducting PVK by a nanoprecipitation method[23,43,44] in a THF/ethanol mixture containing PVP polymers, as shown in Figure 2. PVK is insoluble in high-polarity solvents such as ethanol. When the mixed solution of PVK and MSN-EuLC particles in THF was injected to the solution of PVP in ethanol, the sudden increase in the ethanol/THF ratio led to the collapse of PVK polymer chains and, in turn, the precipitation of PVK on the solid surfaces of the particles.[21] PVP was employed as a surfactant to stabilize the obtained MSN-EuLC@PVK particles with hydrophobic surface.

Typical TEM and SEM images of the as-prepared MSN-EuLC@PVK-PVP are shown in Figure 3c,d. It is noteworthy that the open mesopore structures of MSN-EuLC@PVK-PVP could not be identified, as revealed by the dramatically reduced brightness in the particles from the TEM image. This implies that the mesopores were blocked/sealed during the polymer

encapsulation process. A notable change in the particle morphology and surface roughness can be identified in the SEM image, indicative of the polymer coating. The BET surface area decreased sharply to 50 m^2/g, and the capillary condensation of nitrogen from the mesopores disappeared in the nitrogen sorption isotherm (Figure 4c,d). Additionally, the peak in the small angle XRD pattern becomes negligible, affirming that the mesopores were blocked by the polymer coating. In contrast, no discernible differences can be observed for the synthesis in the absence of PVK (MSN-EuLC with physically adsorbed PVP), as revealed by the corresponding TEM image (Figure S3 of the Supporting Information). Therefore, it is confirmed that the nanoprecipitation process successfully induced the encapsulation of PVK polymers on MSN-EuLC particles. In the FT-IR spectrum, the organic matter's typical C−H stretching vibrations centered at 2925 and 2857 cm^{-1} were greatly enhanced (Figure 4b), which is in good agreement with a weight loss of ∼50 wt % in the TGA curve (Figure 4a). Moreover, the broad band centered at around 3470−3450 cm^{-1}, corresponding to the overlapping of the O−H stretching bands of hydrogen-bonded water molecules and SiO−H stretching of surface silanols hydrogen-bonded to water,[45] significantly diminished in the case of MSN-EuLC@PVK-PVP, possibly due to the increase in the refractive index and/or the elimination of hydrogen-bonded water by the polymer coating.

The success of PVK encapsulation on MSN-EuLC is most likely related to the affinity between NTA and PVK originated from the hydrophobic aromatic rings in their molecular structures, because the π-conjugated structures of the semiconducting polymer can densely pack aromatic molecules by $\pi-\pi$ stacking and hydrophobic interactions.[46−48] As the Eu^{3+} complex is water insoluble, uncharged, and has a low molecular weight, it has similar physical properties to some hydrophobic drugs.[49] Already in an early report, Chiu and co-workers have demonstrated that Eu complex can be easily doped in semiconducting polymer dots formed by a similar nanoprecipitation process.[21] We found that the MSN-EuLC particles can only be readily dispersed in low-polarity organic solvents with a peak at ∼450 nm in the hydrodynamic diameter distribution determined by DLS (Figure S4 of the Supporting Information). It was very hard to obtain a size distribution curve in water due to a fast aggregation and sedimentation of the sample. However, MSN-EuLC@PVK-PVP displays a narrow peak (610 nm) in its hydrodynamic diameter distribution, indicative of the successful stabilization of the hybrid particles by PVP. Moreover, no MSN-free PVK particles were found, as the result of heterogeneous nucleation is energetically favored over the formation of new PVK dots through the homogeneous nucleation.[44] However, particle agglomeration or MSN-free polymer particles was found when the synthesis was performed at higher PVK concentrations (Figure S5 of the Supporting Information), revealing the lack of the controllability in polymer precipitation in the presence of excessive PVK.

Photophysical Studies. The UV absorption spectra of MSN-EuLC and MSN-EuLC@PVP-PVK in ethanol are shown in Figure 5a. The maximum absorption band at ∼334 nm is attributed to singlet−singlet $\pi-\pi^*$ enol absorption of the β-diketonate. PVK encapsulation led to the rise of typical absorption peaks of PVK at 294 and 345 nm. Figure 5b shows the room-temperature excitation and emission spectra of MSN-EuLC and MSN-EuLC@PVP-PVK in different solvents. The

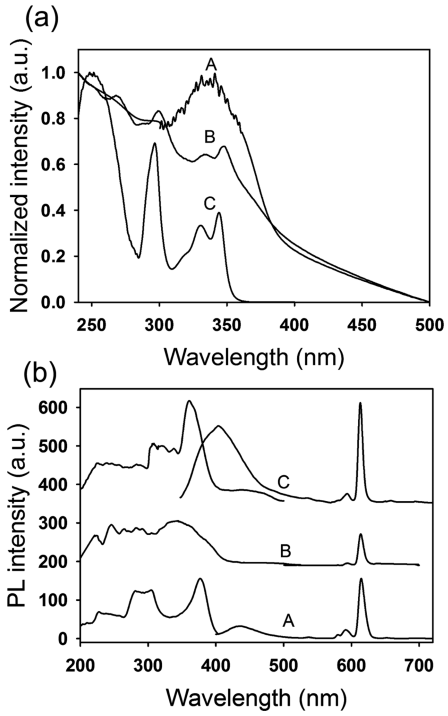

Figure 5. (a) UV absorption spectra of MSN-EuLC in ethanol (A), MSN-EuLC@PVK-PVP in HEPES buffer (B), and PVK in THF (C). (b) Luminescence excitation and emission spectra of MSN-EuLC in ethanol (A), MSN-EuLC in HEPES (pH 7.2, 25 mM) buffer (B), and MSN-EuLC@PVK-PVP in HEPES buffer (C). The excitation spectra were all collected by monitoring the strongest emission wavelength of the Eu^{3+} ions at 615 nm. The same particle concentration of 0.1 mg/mL was used in the measurements. The spectra were shifted for clarity.

excitation spectra of all materials exhibit a broad and intense band between 200 and 400 nm, which is characteristic of the "antenna effect", i.e., the absorption in the NTA-Si ligand and the energy transfer to the Eu^{3+} emitting levels.[3] The characteristic intra-$4f^6$ Eu^{3+} transitions from the $^5D_0$ to ^7F_J (J = 0−4) levels are identified as follows: $^5D_0$ to $^7F_0$ (581 nm), $^5D_0$ to $^7F_1$ (593 nm), $^5D_0$ to $^7F_2$ (615 nm), $^5D_0$ to $^7F_3$ (653 nm), $^5D_0$ to $^7F_4$ (697 nm). The transition of $^5D_0$ to $^7F_2$ is purely electric dipolar, and its high intensity of the hypersensitive transition means that the site occupied by the Eu^{3+} ion is not centrosymmetrical and that the ligand field is strongly polarizing.

The excitation maximum for MSN-EuLC is 378 nm in ethanol and shifted to 342 nm in HEPES buffer (pH 7.2). A new peak at a shorter wavelength of 302 nm was also found in the absorption spectrum of MSN-EuLC in HEPES. Such water-induced shifts are most likely due to the solvation interactions between the polar groups (enol of the β-diketonate) bound to the Eu center and water, which was found in lanthanide complex systems.[50] The interactions mainly depend on the high polarity of water and hydrogen-bond, and may subsequently cause changes in the $\pi-\pi^*$ state energy of the ligands and the first coordination sphere of Eu center, as well as partial decomposition of the complexes resulting in the release of free ligands.[51] Interestingly, there is another absorption peak at 346 nm for MSN-EuLC in HEPES buffer, revealing a red shift compared with the spectrum in ethanol. The red shift is possibly a consequence of solvent effects through the higher

stabilization of the S1 excited state of the released NTA ligands in a much more polar solvent like water.

The emission maximum at 615 nm for MSN-EuLC was reduced by ~2 times in HEPES buffer, as compared with that in ethanol. These results are in agreement with the previous studies.[3,4] Water molecules can play a crucial role of quenching oscillators if Europium centers are not protected against the influence of the species in the environmental solution.[3,4] However, after MSN-EuLC particles were encapsulated by PVK, the emission maximum at 615 nm was increased by ~2.5 times in HEPES buffer, in marked contrast to pure MSN-EuLC. The enhancement is presumably related to the efficient protection of Europium centers from vibronic quenching by energy transfer to OH (i.e., nearby or coordinated water molecules) in aqueous media.[52−54] It has also been proven by a recent study that a hydrophobic atmosphere inside nanoparticles can strip coordinating water molecules from the first coordination sphere of the Eu(III) complex accumulated in nanoparticles.[54] In our particle system, it is the PVK polymer shell that efficiently removes luminescence-quenching water from the vicinity of the complexes by producing a hydrophobic environment. As confirmed by nitrogen sorption, the precipitated PVK polymers on the outer surface of MSN-EuLC sealed the Europium complexes that are on the surfaces of the mesopore walls. Besides, the emission peak of pure PVK centered at 400 nm overlaps with the excitation spectrum of NTA ligand (Figure S6 of the Supporting Information), which made it possible for Föster resonance energy transfer (FRET) to take place between the donor PVK and the acceptor Eu complexes inside MSN-EuLC.[21] However, a blue emission band with a maximum at ~400 nm is observed in the emission spectrum of MSN-EuLC@PVK-PVP (curve C of Figure 5b), indicating the presence of emission from PVK polymers in the composite particles. Due to the confinement of Europium complexes in the pore space and the proximity prerequisite of FRET pairs, only the PVK polymers inside the mesopores or close to the external silica surface can act as luminescence donors for transferring the energy to NTA. Consequently, the PVK molecules in the outer layer of MSN-EuLC@PVK-PVP were left for individual fluorescence when excited.

The $^5D_0$ lifetime values (τ_{obs}) of MSN-EuLC and MSN-EuLC@PVK-PVP were determined from the corresponding luminescence decay profiles (room temperature, Figure 6). All of the decay curves were well reproduced by a single exponential function, and the lifetimes listed in Table 2 were obtained. The $^5D_0$ excited-state lifetime of MSN-EuLC in HEPES (0.28 ms) is shorter than that in ethanol (0.38 ms). These low lifetime values are associated with the quenching by OH group oscillators from the water molecules in the aqueous media. The encapsulation of MSN-EuLC by PVK results in stronger emission (Figure 6 inset) and longer luminescence lifetime (0.51 ms). The other photoluminescence parameters, including intensity ratio of the electric dipole transition to the magnetic dipole transition (I_{02}/I_{01}), radiative (k_r) and nonradiative (k_{nr}) decay rates, radiative lifetime (τ_{rad}), intrinsic quantum yield (Φ_{Ln}, %), absolute quantum yield (Φ_{abs}, %), and the energy transfer efficiency (Φ_{trans}, %) for MSN-EuLC in ethanol, MSN-EuLC in HEPES buffer, and MSN-EuLC@PVK-PVP in HEPES buffer, were calculated based on the emission spectra parameters and τ_{obs} by using the methods described in more detail elsewhere (see the Supporting Information), and summarized in Table 2.

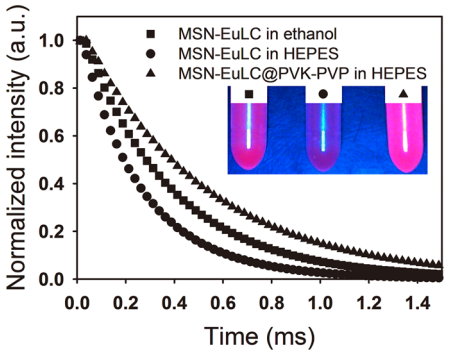

Figure 6. Experimental luminescence decay profiles of MSN-EuLC in ethanol, MSN-EuLC in HEPES buffer, and MSN-EuLC@PVK-PVP in HEPES buffer HEPES (pH 7.2, 25 mM), monitored around 615 nm and excited at their maximum emission wavelengths. The same particle concentration of 0.1 mg/mL was used in the measurements.

Table 2. Intensity Ratio of the Electric Dipole Transition to the Magnetic Dipole Transition ($I(^5D_0$ to $^7F_2)/I(^5D_0$ to $^7F_1)$, I_{02}/I_{01}), Radiative (k_r) and Nonradiative (k_{nr}) Decay Rates, $^5D_0$ Lifetime (τ_{obs}), Radiative Lifetime (τ_{rad}), Intrinsic Quantum Yield (Φ_{Ln}, %), Absolute Quantum Yield (Φ_{abs}, %), and Energy Transfer Efficiency (Φ_{trans}, %) for MSN-EuLC in Ethanol, MSN-EuLC in HEPES Buffer, and MSN-EuLC@PVK-PVP in HEPES Buffer (pH 7.2, 25 mM)[a]

	MSN-EuLC in ethanol	MSN-EuLC in HEPES	MSN-EuLC@PVK-PVP in HEPES
I_{02}/I_{01}	10	8	11
τ_{obs} (ms)	0.38	0.28	0.51
τ_{rad} (ms)	1.28	1.55	1.31
k_r (ms^{-1})	0.78	0.65	0.76
k_{nr} (ms^{-1})	1.86	2.87	1.19
Φ_{Ln} (%)	29	18	39
Φ_{abs} (%)	5.1	1.7	9.3
Φ_{trans} (%)	18	9.4	24

[a]The related methods for calculating these parameters are listed in the Supporting Information.

It is evident that MSN-EuLC@PVK-PVP in HEPES buffer possesses the highest color purity (I_{02}/I_{01} = 11), a large intrinsic quantum yield of Eu^{3+} (39%), and a higher absolute quantum yield (9.3%). For the color purity, it is well-known that the $^5D_0$ to $^7F_2$ transition is a typical electric-dipole transition whereas the $^5D_0$ to $^7F_1$ transition corresponds to a characteristic parity-allowed magnetic dipole transition.[3] The I_{02}/I_{01} ratio measures the symmetry of the coordination sphere, and this ratio provides valuable information about the chemical microenvironment change of ligands coordinating the Eu^{3+} ion. Compared to MSN-EuLC, the I_{02}/I_{01} value of the MSN-EuLC@PVK-PVP particles is the highest. This demonstrates that the local symmetry changed upon encapsulating of MSN-EuLC into PVK polymers and that a more asymmetric environment was occupied by the Eu^{3+} ion, probably due to the protection of the complexes against solvent influence, as well as possible distortion of the symmetry around Eu^{3+} by PVK polymers.[22] Moreover, the nonradiative decay rate (k_{nr}), which depends on the number of quenchers (especially water molecules and ions) present inside the inner coordination sphere of lanthanide ion, is significantly low (1.19 ms^{-1}) for

MSN-EuLC@PVK-PVP, implying an increased excited state population by minimizing nonradiative pathways. Owing to the PVK encapsulation, vibration transition under the influences from the environment is suppressed because of the protection from the impermeable PVK layer. As a consequence, more energy is transferred from the organic ligands to Eu^{3+} (Φ_{trans}, 24%), leading to improvement of the photoluminescence.

Measurements of photoluminescence intensity in various aqueous media were then conducted to investigate the stability of Europium complexes in different particles. As shown in Figure 7a, MSN-EuLC@PVK-PVP can emit intense luminescence under UV radiation over a wide pH range of 4−9 without significant reduction. In contrast, the luminescence intensity of MSN-EuLC is the highest at neutral pH and decreased notably in both acidic and basic conditions. This is in line with the previous findings that the luminescence of lanthanide complex in aqueous media can be reduced by ion quenching or replacement.[18,55] Further comparison of luminescence in different biologically relevant aqueous media is shown in Figure 7b. The quenching for MSN-EuLC in PBS buffer, Dulbecco's modified Eagle's medium (DMEM) cell medium, and DMEM in the presence of 10% FBS (fetal bovine serum) was much more significant than that in pure water. Particularly, in DMEM and DMEM in the presence of 10% FBS, the luminescence intensity is extremely low, indicative of strong quenching. Apparently, the stability of Europium complexes in MSN-EuLC was not strong enough to prevent the particles from quenching in complicated biological media containing large amount of ions, solvents, proteins, etc. Conversely, PVK encapsulated particles are superior in maintaining the luminescence in different aqueous media. We then proceeded to further check their photostability by continuous excitation of the HEPES suspension of MSN-EuLC@PVK-PVP for up to 30 min. The photoluminescence was maintained, indicating high photostability (Figure S7 of the Supporting Information).

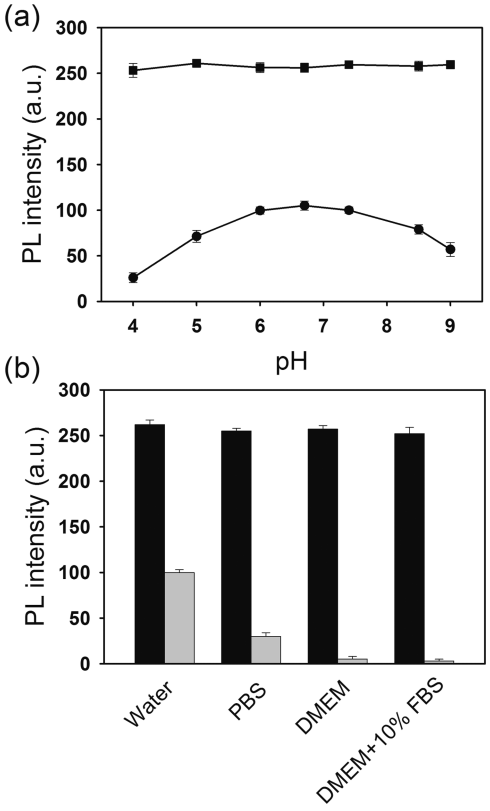

Figure 7. Photoluminescence intensity comparison of (a) MSN-EuLC (circle) and MSN-EuLC@PVK-PVP (square) at different pH values, (b) MSN-EuLC (gray) and MSN-EuLC@PVK-PVP (dark) in different biologically relevant media. Intensities were determined at around 615 nm and excited at their maximum emission wavelengths.

The unique property of having a long luminescence lifetime distinguishes Eu complex from other fluorophores emitting red fluorescence. Typical time-resolved luminescent images of MSN-EuLC particles and MSN-EuLC@PVK-PVP particles are displayed in Figure 8. The Europium complexes could be imaged with high signal and nonexistent background signal in this time-resolved microscopy setup, because they emitted photons after a delay time of 600 μs.[31,32] Encouragingly, when regions of a similar particle density were imaged, MSN-EuLC@PVK-PVP particles show much higher luminescence brightness and a high amount of uniform bright dots that could be seen as individual particles, as well as some larger aggregates. This demonstrated the high intrinsic quantum yield, long luminescence lifetime of Eu^{3+}, and high stability in the novel composites. In contrast, the photoluminescent signal from MSN-EuLC particles was nearly 1 order of magnitude weaker, and most of the particles are hard to discern, leaving only large aggregates visible.

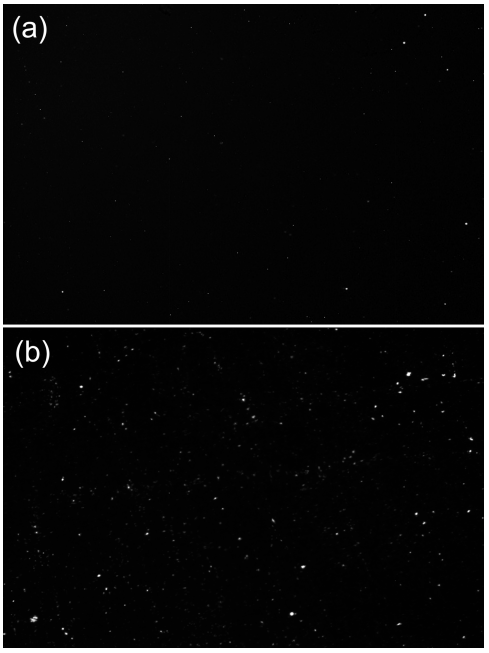

Figure 8. Time-resolved luminescent images of MSN-EuLC particles (a), and MSN-EuLC@PVK-PVP particles (b). The samples were prepared on glass microscope slides by drying the corresponding solutions in HEPES buffer HEPES (pH 7.2, 25 mM) with the same particle concentration (0.1 mg/mL). The delay time (between the termination of excitation illumination and start of luminescence signal collection), the gate time (luminescence signal collection time after one illumination pulse), and the integration time (total luminescence signal collection time) for the measurements were 600, 800 μs, and 30 s, respectively.

CONCLUSIONS

This work presents the possibility of employing semiconducting polymers to encapsulate lanthanide complex immobilized

mesoporous hosts for bright and stable photoluminescence in aqueous media. Luminescent Eu^{3+} complexes were covalently immobilized in the ordered mesoporous silica particles by bridging via the monosilylated NTA ligands (NTA-Si) co-condensed in the silica network. Albeit with a bimodal pore size distribution with two peaks at 3.5 and 5.3 nm, the prepared MSN-NTA particles exhibit a high NTA-Si functionalization degree (0.42 mmol/g), which was facilitated by using 2-propanol as a cosolvent in the synthesis. The Europium complexation was conducted on the as-obtained MSN-NTA particles with an average diameter of ∼450 nm, followed by encapsulation of hydrophobic semiconducting PVK polymers through solvent induced surface precipitation. Stabilized by PVP polymer, the final organic−inorganic composite material (MSN-EuLC@PVK-PVP) possesses good dispersibility in water. Investigations of luminescence properties show that MSN-EuLC@PVK-PVP particles exhibit significantly higher quantum yield (Φ_{Ln} = 39%, Φ_{abs} = 9.3%), and longer lifetime (τ_{obs} = 0.51 ms), as compared with those without polymer encapsulation. Most importantly, a high luminescence stability was realized when MSN-EuLC@PVK-PVP particles were dispersed in various aqueous media, showing no measurable quenching effect. Thus, the PVK encapsulation efficiently removes luminescence-quenching water from the vicinity of the complexes by creating a hydrophobic environment. The presented hybrid material may break through the current limitations of applying lanthanide-doped hybrid organic−inorganic materials in dry form for luminescent displays or in simple aqueous solution for biosensors only. The results presented here are thus a promising step in exploiting the possibility of using mesoporous particles immobilized with emitting lanthanide centers in complex aqueous environments for possible applications such as time-resolved luminescent imaging also under biological/physiological conditions.

■ ASSOCIATED CONTENT

Supporting Information

^{1}H NMR spectra of the as-synthesized monosilylated NTA ligand (NTA-Si), and FT-IR spectra comparison of NTA and NTA-Si, TEM images and nitrogen sorption isotherms of MSN-NTA particles synthesized with methanol and ethanol as the organic solvents, TEM image of MSN-EuLC particles anchored with Eu^{3+} complex and MSN-EuLC particles with physically adsorbed PVP (MSN-EuLC@PVK-PVP synthesis in the absence of PVK, hydrodynamic size distributions of MSN-EuLC in ethanol and MSN-EuLC@PVK-PVP in HEPES buffer (pH 7.2, 25 mM), TEM image of MSN-EuLC@PVK-PVP particles synthesized with higher PVK concentration of 3 and 5 mg/mL while keeping the other synthetic parameters the same, photoluminescent excitation and emission spectra of PVK and NTA in THF, photoluminescence intensity at 615 nm as a function of irradiation time (excitation wavelength 360 nm) for 0.1 mg/mL of MSN-EuLC@PVK suspension in HEPES buffer (25 mM, pH 7.2), and calculation of photoluminescence parameters. This material is available free of charge via the Internet at http://pubs.acs.org.

■ AUTHOR INFORMATION

Corresponding Authors

*J. Zhang. Tel.: +86 2365102507. E-mail: jixizhang@cqu.edu.cn.

*J. M. Rosenholm. Tel.: +358 2215 3255. E-mail: jerosenh@abo.fi.

Author Contributions

All authors have given approval to the final version of the paper.

Notes

The authors declare no competing financial interest.

■ ACKNOWLEDGMENTS

The financial support by the Magnus Ehrnrooth Foundation (J.Z.), the Maud Kuistila Memorial Foundation (J.Z.), Doctoral Education Network in Material Research (N.P.) at Åbo Akademi University, Finland, and The Academy of Finland projects #260599 (J.Z., N.P., J.M.R.) and 278812 (J.M.R.) are greatly acknowledged. Docent Patrik Eklund from Laboratory of Organic Chemistry, Process Chemistry Centre, Åbo Akademi University is acknowledged for the NMR characterizations. We also acknowledge the assistance by Markus Peurla from University of Turku during the TEM characterization, as well as the help by Riikka Arppe from University of Turku during the determination of the luminescence lifetimes.

■ REFERENCES

(1) Feng, J.; Zhang, H. Hybrid Materials Based on Lanthanide Organic Complexes: A Review. *Chem. Soc. Rev.* **2013**, *42*, 387−410.

(2) Bünzli, J.-C. G. Lanthanide Luminescence for Biomedical Analyses and Imaging. *Chem. Rev.* **2010**, *110*, 2729−2755.

(3) Binnemans, K. Lanthanide-based Luminescent Hybrid Materials. *Chem. Rev.* **2009**, *109*, 4283−4374.

(4) Escribano, P.; Julian-Lopez, B.; Planelles-Arago, J.; Cordoncillo, E.; Viana, B.; Sanchez, C. Photonic and Nanobiophotonic Properties of Luminescent Lanthanide-Doped Hybrid Organic-Inorganic Materials. *J. Mater. Chem.* **2008**, *18*, 23−40.

(5) He, Q.; Shi, J. MSN Anti-Cancer Nanomedicines: Chemotherapy Enhancement, Overcoming of Drug Resistance, and Metastasis Inhibition. *Adv. Mater.* **2014**, *26*, 391−411.

(6) Yang, P.; Gai, S.; Lin, J. Functionalized Mesoporous Silica Materials for Controlled Drug Delivery. *Chem. Soc. Rev.* **2012**, *41*, 3679−3698.

(7) Rosenholm, J. M.; Mamaeva, V.; Sahlgren, C.; Lindén, M. Nanoparticles in Targeted Cancer Therapy: Mesoporous Silica Nanoparticles Entering Preclinical Development Stage. *Nanomedicine* **2012**, *7*, 111−120.

(8) Yan, B.; Li, Y. Luminescent Ternary Inorganic-Organic Mesoporous Hybrids Eu(TTASi-SBA-15)Phen: Covalent Linkage in TTA Directly Functionalized SBA-15. *Dalton Trans.* **2010**, *39*, 1480−1487.

(9) Li, Y.; Yan, B. Photoactive Europium(III) Centered Mesoporous Hybrids with 2-Thenoyltrifluoroacetone Functionalized SBA-16 and Organic Polymers. *Dalton Trans.* **2010**, *39*, 2554−2562.

(10) Feng, J.; Song, S.-Y.; Fan, W.-Q.; Sun, L.-N.; Guo, X.-M.; Peng, C.-Y.; Yu, J.-B.; Yu, Y.-N.; Zhang, H.-J. Near-Infrared Luminescent Mesoporous MCM-41 Materials Covalently Bonded with Ternary Thulium Complexes. *Microporous Mesoporous Mater.* **2009**, *117*, 278−284.

(11) Bruno, S. M.; Ferreira, R. A. S.; Almeida Paz, F. A.; Carlos, L. s. D.; Pillinger, M.; Ribeiro-Claro, P.; Gonçalves, I. S. Structural and Photoluminescence Studies of a Europium(III) Tetrakis(β-Diketonate) Complex with Tetrabutylammonium, Imidazolium, Pyridinium and Silica-Supported Imidazolium Counterions. *Inorg. Chem.* **2009**, *48*, 4882−4895.

(12) Ambili Raj, D. B.; Biju, S.; Reddy, M. L. P. Highly Luminescent Europium(III) Complexes Containing Organosilyl 4,4,5,5,5-Pentafluoro-1-(naphthalen-2-yl)pentane-1,3-dionate Ligands Grafted on Silica Nanoparticles. *J. Mater. Chem.* **2009**, *19*, 7976−7983.

(13) DeOliveira, E.; Neri, C. R.; Serra, O. A.; Prado, A. G. S. Antenna Effect in Highly Luminescent Eu^{3+} Anchored in Hexagonal Mesoporous Silica. *Chem. Mater.* **2007**, *19*, 5437−5442.

(14) Sun, L.-N.; Zhang, H.-J.; Peng, C.-Y.; Yu, J.-B.; Meng, Q.-G.; Fu, L.-S.; Liu, F.-Y.; Guo, X.-M. Covalent Linking of Near-Infrared

Luminescent Ternary Lanthanide (Er^{3+}, Nd^{3+}, Yb^{3+}) Complexes on Functionalized Mesoporous MCM-41 and SBA-15. *J. Phys. Chem. B* **2006**, *110*, 7249−7258.
(15) Li, Y.; Yan, B.; Yang, H. Construction, Characterization, and Photoluminescence of Mesoporous Hybrids Containing Europium(III) Complexes Covalently Bonded to SBA-15 Directly Functionalized by Modified β-Diketone. *J. Phys. Chem. C* **2008**, *112*, 3959−3968.
(16) Guo, X.; Guo, H.; Fu, L.; Deng, R.; Chen, W.; Feng, J.; Dang, S.; Zhang, H. Synthesis, Spectroscopic Properties, and Stabilities of Ternary Europium Complex in SBA-15 and Periodic Mesoporous Organosilica: A Comparative Study. *J. Phys. Chem. C* **2009**, *113*, 2603−2610.
(17) Li, Y.-J.; Yan, B. Lanthanide (Eu^{3+}, Tb^{3+})/β-Diketone Modified Mesoporous SBA-15/Organic Polymer Hybrids: Chemically Bonded Construction, Physical Characterization, and Photophysical Properties. *Inorg. Chem.* **2009**, *48*, 8276−8285.
(18) Leonard, J. P.; dos Santos, C. M. G.; Plush, S. E.; McCabe, T.; Gunnlaugsson, T. pH Driven Self-Assembly of a Ternary Lanthanide Luminescence Complex: The Sensing of Anions Using a β-Diketonate-Eu(iii) Displacement Assay. *Chem. Commun.* **2007**, 129−131.
(19) Blair, S.; Lowe, M. P.; Mathieu, C. E.; Parker, D.; Senanayake, P. K.; Kataky, R. Narrow-Range Optical pH Sensors Based on Luminescent Europium and Terbium Complexes Immobilized in a Sol Gel Glass. *Inorg. Chem.* **2001**, *40*, 5860−5867.
(20) Ai, K.; Zhang, B.; Lu, L. Europium-based Fluorescence Nanoparticle Sensor for Rapid and Ultrasensitive Detection of an Anthrax Biomarker. *Angew. Chem., Int. Ed.* **2009**, *48*, 304−308.
(21) Sun, W.; Yu, J.; Deng, R.; Rong, Y.; Fujimoto, B.; Wu, C.; Zhang, H.; Chiu, D. T. Semiconducting Polymer Dots Doped with Europium Complexes Showing Ultranarrow Emission and Long Luminescence Lifetime for Time-Gated Cellular Imaging. *Angew. Chem., Int. Ed.* **2013**, *52*, 11294−11297.
(22) Raj, D. B. A.; Francis, B.; Reddy, M. L. P.; Butorac, R. R.; Lynch, V. M.; Cowley, A. H. Highly Luminescent Poly(methyl methacrylate)-Incorporated Europium Complex Supported by a Carbazole-based Fluorinated β-Diketonate Ligand and a 4,5-Bis(diphenylphosphino)-9,9-dimethylxanthene Oxide Co-Ligand. *Inorg. Chem.* **2010**, *49*, 9055−9063.
(23) Wu, C.; Chiu, D. T. Highly Fluorescent Semiconducting Polymer Dots for Biology and Medicine. *Angew. Chem., Int. Ed.* **2013**, *52*, 3086−3109.
(24) Chan, Y.-H.; Ye, F.; Gallina, M. E.; Zhang, X.; Jin, Y.; Wu, I. C.; Chiu, D. T. Hybrid Semiconducting Polymer Dot−Quantum Dot with Narrow-Band Emission, Near-Infrared Fluorescence, and High Brightness. *J. Am. Chem. Soc.* **2012**, *134*, 7309−7312.
(25) Zhang, J.; Niemela, M.; Westermarck, J.; Rosenholm, J. M. Mesoporous Silica Nanoparticles with Redox-Responsive Surface Linkers for Charge-Reversible Loading and Release of Short Oligonucleotides. *Dalton Trans.* **2014**, *43*, 4115−4126.
(26) Lang, N.; Tuel, A. A Fast and Efficient Ion-Exchange Procedure to Remove Surfactant Molecules from MCM-41 Materials. *Chem. Mater.* **2004**, *16*, 1961−1966.
(27) Rosenholm, J. M.; Lindén, M. Wet-Chemical Analysis of Surface Concentration of Accessible Groups on Different Amino-Functionalized Mesoporous SBA-15 Silicas. *Chem. Mater.* **2007**, *19*, 5023−5034.
(28) Brunauer, S.; Emmett, P. H.; Teller, E. Adsorption of Gases in Multimolecular Layers. *J. Am. Chem. Soc.* **1938**, *60*, 309−319.
(29) Ravikovitch, P. I.; Wei, D.; Chueh, W. T.; Haller, G. L.; Neimark, A. V. Evaluation of Pore Structure Parameters of MCM-41 Catalyst Supports and Catalysts by Means of Nitrogen and Argon Adsorption. *J. Phys. Chem. B* **1997**, *101*, 3671−3679.
(30) Hakala, H.; Liitti, P.; Peuralahti, J.; Karvinen, J.; Mukkala, V.-M.; Hovinen, J. Development of Luminescent Sm(III) Chelates Containing Hexadentate to Nonadentate Ligands: Synthesis, Photophysical Properties and Coupling to Biomolecules. *J. Lumin.* **2005**, *113*, 17−26.
(31) Huttunen, R. J.; O'Riordan, T. C.; Härkönen, P. L.; Soini, J. T.; Meltola, N. J.; Hänninen, P. E.; Soini, A. E. Quantitative Detection of Cell Surface Protein Expression by Time-Resolved Fluorimetry. *Luminescence* **2007**, *22*, 163−170.
(32) Soini, A. E.; Kuusisto, A.; Meltola, N. J.; Soini, E.; Seveus, L. A New Technique for Multiparameter Imaging Microscopy: Use of Long Decay Time Photoluminescent Labels Enables Multiple Color Immunocytochemistry with Low Channel-to-Channel Crosstalk. *Microsc. Res. Technol.* **2003**, *62*, 396−407.
(33) Liu, J.; Yang, J.; Yang, Q.; Wang, G.; Li, Y. Hydrothermally Stable Thioether-Bridged Mesoporous Materials with Void Defects in the Pore Walls. *Adv. Funct. Mater.* **2005**, *15*, 1297−1302.
(34) Díaz, I.; Pérez-Pariente, J. Synthesis of Spongelike Functionalized MCM-41 Materials from Gels Containing Amino Acids. *Chem. Mater.* **2002**, *14*, 4641−4646.
(35) Linares, N.; Serrano, E.; Rico, M.; Mariana Balu, A.; Losada, E.; Luque, R.; Garcia-Martinez, J. Incorporation of Chemical Functionalities in the Framework of Mesoporous Silica. *Chem. Commun.* **2011**, *47*, 9024−9035.
(36) Huh, S.; Wiench, J. W.; Yoo, J.-C.; Pruski, M.; Lin, V. S. Y. Organic Functionalization and Morphology Control of Mesoporous Silicas Via a Co-Condensation Synthesis Method. *Chem. Mater.* **2003**, *15*, 4247−4256.
(37) Eriksson, J. C.; Gillberg, G. NMR-Studies of the Solubilisation of Aromatic Compounds in Cetyltrimethylammonium Bromide Solution. II. *Acta Chem. Scand.* **1966**, *20*, 2019−2027.
(38) Zhang, D.; Tang, D.; Wang, X.; Qiao, Z.-a.; Li, Y.; Liu, Y.; Huo, Q. Preparation of Hybrid Mesoporous Silica Luminescent Nanoparticles with Lanthanide(III) Complexes and Their Exhibition of White Emission. *Dalton Trans.* **2011**, *40*, 9313−9319.
(39) Zhang, D.; Wang, X.; Qiao, Z.-a.; Tang, D.; Liu, Y.; Huo, Q. Synthesis and Characterization of Novel Lanthanide(III) Complexes-Functionalized Mesoporous Silica Nanoparticles as Fluorescent Nanomaterials. *J. Phys. Chem. C* **2010**, *114*, 12505−12510.
(40) Sun, L.-N.; Zhang, H.-J.; Yu, J.-B.; Yu, S.-Y.; Peng, C.-Y.; Dang, S.; Guo, X.-M.; Feng, J. Near-Infrared Emission from Novel Tris(8-hydroxyquinolinate)lanthanide(III) Complexes-Functionalized Mesoporous SBA-15. *Langmuir* **2008**, *24*, 5500−5507.
(41) Ma, B.-Q.; Gao, S.; Yi, T.; Xu, G.-X. One-Dimensional Coordination Polymers [Co(Acac)2pz]N and [Co(Acac)2(4,4′-Bipy)]N (Acac=Acetylacetone, Pz=Pyrazine, Bipy=4,4′-Bipyridine): Synthesis, Structures and Magnetic Properties. *Polyhedron* **2001**, *20*, 1255−1261.
(42) Ottaviani, M. F.; Moscatelli, A.; Desplantier-Giscard, D.; Di Renzo, F.; Kooyman, P. J.; Alonso, B.; Galarneau, A. Synthesis of Micelle-Templated Silicas from Cetyltrimethylammonium Bromide/1,3,5-Trimethylbenzene Micelles. *J. Phys. Chem. B* **2004**, *108*, 12123−12129.
(43) Fang, R. H.; Aryal, S.; Hu, C.-M. J.; Zhang, L. Quick Synthesis of Lipid−Polymer Hybrid Nanoparticles with Low Polydispersity Using a Single-Step Sonication Method. *Langmuir* **2010**, *26*, 16958−16962.
(44) Dudnik, V.; Sukhorukov, G. B.; Radtchenko, I. L.; Möhwald, H. Coating of Colloidal Particles by Controlled Precipitation of Polymers. *Macromolecules* **2001**, *34*, 2329−2334.
(45) Innocenzi, P. Infrared Spectroscopy of Sol−Gel Derived Silica-based Films: A Spectra-Microstructure Overview. *J. Non-Cryst. Solids* **2003**, *316*, 309−319.
(46) Chen, Z.; Fimmel, B.; Wurthner, F. Solvent and Substituent Effects on Aggregation Constants of Perylene Bisimide π-Stacks - A Linear Free Energy Relationship Analysis. *Org. Biomol. Chem.* **2012**, *10*, 5845−5855.
(47) Jin, Y.; Ye, F.; Zeigler, M.; Wu, C.; Chiu, D. T. Near-Infrared Fluorescent Dye-Doped Semiconducting Polymer Dots. *ACS Nano* **2011**, *5*, 1468−1475.
(48) Grimland, J. L.; Wu, C.; Ramoutar, R. R.; Brumaghim, J. L.; McNeill, J. Photosensitizer-Doped Conjugated Polymer Nanoparticles with High Cross-Sections for One- and Two-Photon Excitation. *Nanoscale* **2011**, *3*, 1451−1455.

(49) Cui, J.; Wang, Y.; Hao, J.; Caruso, F. Mesoporous Silica-Templated Assembly of Luminescent Polyester Particles. *Chem. Mater.* **2009**, *21*, 4310−4315.
(50) Fantacci, S.; De Angelis, F.; Selloni, A. Absorption Spectrum and Solvatochromism of the [Ru(4,4′-COOH-2,2′-Bpy)2(NCS)2] Molecular Dye by Time Dependent Density Functional Theory. *J. Am. Chem. Soc.* **2003**, *125*, 4381−4387.
(51) Feau, C.; Klein, E.; Dosche, C.; Kerth, P.; Lebeau, L. Synthesis and Characterization of Coumarin-Based Europium Complexes and Luminescence Measurements in Aqueous Media. *Org. Biomol. Chem.* **2009**, *7*, 5259−5270.
(52) Li, P.; Wang, Y.; Li, H.; Calzaferri, G. Luminescence Enhancement after Adding Stoppers to Europium(III) Nanozeolite L. *Angew. Chem., Int. Ed.* **2014**, *53*, 2904−2909.
(53) Zhang, J.; Liu, Y.; Li, Y.; Zhao, H.; Wan, X. Hybrid Assemblies of Eu-Containing Polyoxometalates and Hydrophilic Block Copolymers with Enhanced Emission in Aqueous Solution. *Angew. Chem., Int. Ed.* **2012**, *51*, 4598−4602.
(54) Morikawa, M.-a.; Tsunofuri, S.; Kimizuka, N. Controlled Self-Assembly and Luminescence Characteristics of Eu(III) Complexes in Binary Aqueous/Organic Media. *Langmuir* **2013**, *29*, 12930−12935.
(55) Stanimirov, S.; Petkov, I. Novel pH Responsive Luminescent Poly(oxyethylene phosphate) Tris(β-diketonate) Europium(III) Complexes. *Cent. Eur. J. Chem.* **2008**, *6*, 429−437.